Differential Modulating Effect of MoS_2 on Amyloid Peptide Assemblies

Jie Wang,[a, c] Lei Liu,*[a] Daohan Ge,[d] Hongxing Zhang,[a] Yonghai Feng,[a] Yibang Zhang,[b] Menglin Chen,[c] and Mingdong Dong*[c]

Abstract: The abnormal fibrillogenesis of amyloid peptides such as amyloid fibril and senior amyloid plaques, is associated with the pathogenesis of many amyloid diseases. Hence, modulation of amyloid assemblies is related to the possible pathogenesis of some diseases. Some two-dimensional nanomaterials, that is, graphene oxide, tungsten disulfide, exhibit strong modulation effects on the amyloid fibrillogenesis. Herein, the modulation effect of molybdenum disulfide on two amyloid peptide assemblies based on the label-free techniques is presented, including quartz crystal microbalance (QCM), AFM, and CD spectroscopy. MoS_2 presents different modulating effects on the assembly of amyloid-β peptide (33–42) [Aβ (33–42)] and amylin (20–29), mainly owing to the distinct affinity between amyloid peptides and MoS_2. This is to our knowledge the first report of MoS_2 as a modulator for amyloid aggregation. It enriches the variety of 2D nanomodulators of amyloid fibrillogenesis and explains the mechanism for the self-assembly of amyloid peptides, and expands the applications of MoS_2 in biology.

Amyloid protein misfolding and its irreversible fibril deposits are considered as the main cause associated with many types of diseases, such as Alzheimer's diseases (AD) and type-II diabetes. In the fibrillization process, amyloid peptides aggregate from soluble unstructured monomers into β-sheet-rich oligomers and protofibrils, and finally turn into insoluble amyloid fibril plaques.[1] Since the cytotoxicity of amyloid peptide is mainly related with the aggregates of β-sheet-rich structure, it is rational that a modulator which can reduce, inhibit, or even reverse the fibrillization process, would be of great value to explain pathogenesis and its potential therapeutic treatment.

Many researchers focused on the study of the modulators of amyloid fibrillization.[2] So far, several types of effective modulators have been discovered, such as organic- and inorganic nanoparticles, amine-modified polystyrene nanoparticles,[3] peptide motifs,[4,14] and other biomaterials.[5] Recently, carbonaceous materials were reported to show inhibitory effects on amyloid aggregation, such as graphene oxide (GO) with surface mediation effects, dimensionality, and size effects.[6] The discovery of GO modulation effects motivates GO applications in the detection of amyloid aggregates and medical research.[7] These successes with GO have also opened up a new avenue for similar (2D) materials. One important part of newly-emerging 2D materials is transition-metal dichalcogenides (TMDs). Likewise, WS_2 was also reported to show inhibitory effects for amyloidosis and could even be exfoliated by the self-assembly of amyloids.[8] Similar to GO and WS_2, MoS_2 is composed of 2D layers stacked in the vertical direction. Because of the weak van der Waals interactions between the sheets of sulfide atoms, MoS_2 has excellent lubricating properties. MoS_2 could be exfoliated as single layers or few-layered forms and used in photoelectrochemical fields,[9] switchable transistors,[10] and ultrafast photonics.[11] Recently some studies demonstrated that with appropriate modification, MoS_2 could be applied in tissue engineering and biomedicine[12] as biosensors, for gene delivery, and for photothermal therapy (PTT) for cancer. It is implied that MoS_2 could be a promising material in a variety of bio-applications. In the previous work, although it presented the modulating effect of WS_2 and similar 2D nanomaterials on amyloid peptide aggregation, the differential modulating effect of MoS_2 on the assemblies of amyloid peptides remained to be clarified. This would provide the cues of mechanism and impact factors that modulate amyloid peptide assemblies by MoS_2 and reveal the basic requirements of peptide sequences which could be modulated by MoS_2. Herein, we investigate the modulation effect of MoS_2 in the amyloid fibrillization process to further understand the interaction mechanism between MoS_2 and different amyloid peptides.

Traditional techniques utilized to monitor the aggregation process mainly depend on measuring the change of fluorescent spectra upon dye binding. However, most of these dyes are insensitive to the early aggregates of amyloid proteins.

[a] *Dr. J. Wang, Prof. L. Liu, H. X. Zhang, Y. H. Feng*
Institute for Advanced Materials, Jiangsu University
212013 Xuefu Road No. 301, Zhenjiang city, Jinagsu Province (P.R. China)
E-mail: liul@ujs.edu.cn

[b] *Prof. Y. B. Zhang*
Zhang Department of Pharmaceutics, School of Pharmacy
Jiangsu University, 212013 Xuefu Road No. 301
Zhenjiang city, Jinagsu Province (P.R. China)

[c] *Dr. J. Wang, Prof. M. Chen, Prof. M. D. Dong*
Interdisciplinary Nanoscience Center (iNANO)
Aarhus University, 8000 Aarhus C (Denmark)
E-mail: dong@inano.au.dk

[d] *D. H. Ge*
School of Mechanical Engineering, Micro/nano Science and Technology Center, Jiangsu University, 212013 Xuefu Road No. 301
Zhenjiang city, Jinagsu Province (P.R. China)

Supporting information and the ORCID identification number for the author of this article can be found under https://doi.org/10.1002/chem.201704593.

These dyes interact with amyloid peptide in the aggregation process, which interferes with in situ measurements, for example Congo Red and Thioflavin T (ThT).[13] Herein, we combined label-free quartz crystal microbalance (QCM), atomic force microscopy (AFM), and circular dichroism (CD) spectra, to quantitatively explore the modulating effect of MoS_2 on the fibrillization of two amyloid peptides, Aβ (33–42), a key hydrophobic fragment of amyloid protein Aβ (1–42),[14] and amylin (20–29), the fibrillating core fragment of the human islet amyloid polypeptide (hIAPP) involved in type-II diabetes.[15]

We obtained MoS_2 suspensions by hydrothermal treatment of molybdic oxide and KSCN.[16] The morphologies of MoS_2 were nanosheets, which was characterized by AFM and TEM. The height of MoS_2 sheets was measured to be about 0.5 nm, which indicated the presence of monolayer MoS_2 sheets (Figure S1 a, S2 in the Supporting Information). Overall, the characterization on the morphology revealed that the MoS_2 monolayer sheet was dispersed well in an aqueous solution. Furthermore, MoS_2 was characterized by XRD (Figure S1b), and the characteristic peaks are consistent with the literature values.[16] The characteristic Raman peaks of the MoS_2 were at 378 and 404 cm^{-1}, as presented in Raman spectroscopy (Figure S1 c), confirming the thin-layer structure of nanosheets.[17]

AFM was utilized to explore the modulating effect of MoS_2 on amyloid fibril formation. Aβ (33–42) peptide solution (550 μM) incubated without MoS_2 could form dense, large fibrils, with heights exceeding 8 nm (Figure 1 a). When Aβ (33–42) solution (550 μM) was incubated with 0, 25, 50, and 100 μg mL^{-1} MoS_2, as shown in Figure 1 a–d, the amount of fibrils tended to be reduced with the increasing concentration of MoS_2. Peptide molecules stacked on the surface and formed a thin films of 1.7 nm thickness. The measurements of height and width are shown in Figure S3. The "fibril coverage", defined as the area of fibrils divided by the total image area, can quantitatively evaluate the MoS_2-modulating effect on the peptide assembly. As shown in Figure S4, the coverage of fibrils changed from 36.4 ± 2.7%, 30.1 ± 1.6%, 25.4 ± 1.1% to 2.1 ± 0.1%, with MoS_2 at the concentration of 0, 25, 50, and 100 μg mL^{-1}, respectively. The decrease of fibril coverage is almost linear with the increasing concentration of MoS_2, suggesting that MoS_2 has a strong modulation effect on Aβ (33–42) fibril formation. (Figure 1 e).

We further investigated the modulation effect of MoS_2 on the self-assembly of amylin (20–29), which is a core fragment of human islet amyloid polypeptide (hIAPP). Amylin (20–29) solution (550 μM)was incubated with 0, 25, 50, and 100 μg mL^{-1} MoS_2 at 37 °C for 10 h. The mixture was characterized by AFM after 10 h of incubation at 37 °C (Figure 2). The "fibril coverage" was calculated with increasing concentration of MoS_2 from 0 to 100 μg mL^{-1}. The coverage decreased from 33.5 ± 3.7%, 12.1 ± 1.5%, 5.3 + 0.6% to 3.0 + 0.2%. This result shows that MoS_2 is also effective for the inhibition of amylin (20–29) fibrillogenesis. The relationship between the concentration of MoS_2, fibril coverage, and fibril height is presented in Figure S4, which clearly shows that increasing MoS_2 concentration can result in diminishing amyloidosis. The fibril coverage analysis also displayed that the effect of MoS_2 on modulating the fibril-

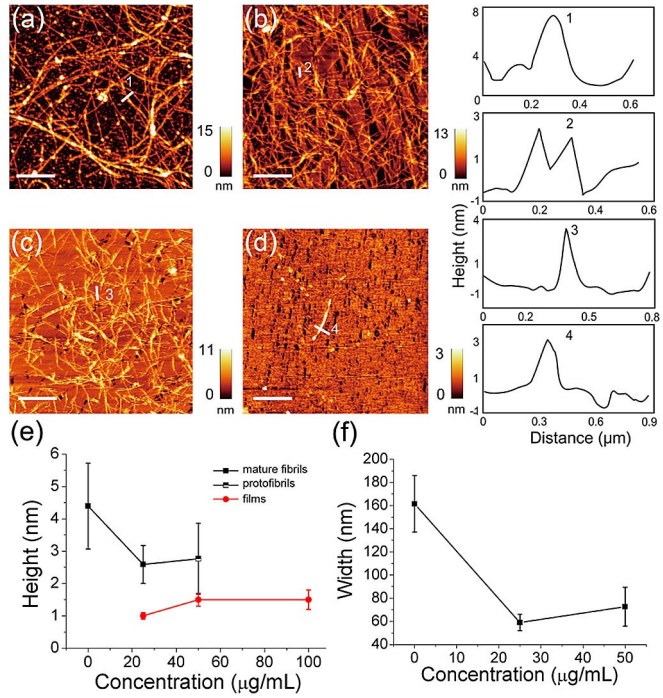

Figure 1. a) AFM images show MoS_2 modulation of Aβ (33–42) aggregation. Aβ (33–42) peptide solution (550 μM) was incubated for 10 h at 37 °C. Aβ (33–42) peptide solution (550 μM) with 25 (b), 50 (c), and 100 (d) μg mL^{-1} MoS_2 incubated for 10 h at 37 °C. The scale bar in the image is 2 μm. The heights of mixture of Aβ (33–42) and MoS_2 were 8.2 ± 1.6, 6.5 ± 1.4, 4 ± 0.3, and 2.3 ± 0.2 nm, respectively. The analyses for the fibril coverage show fibril height (e) and width (f).

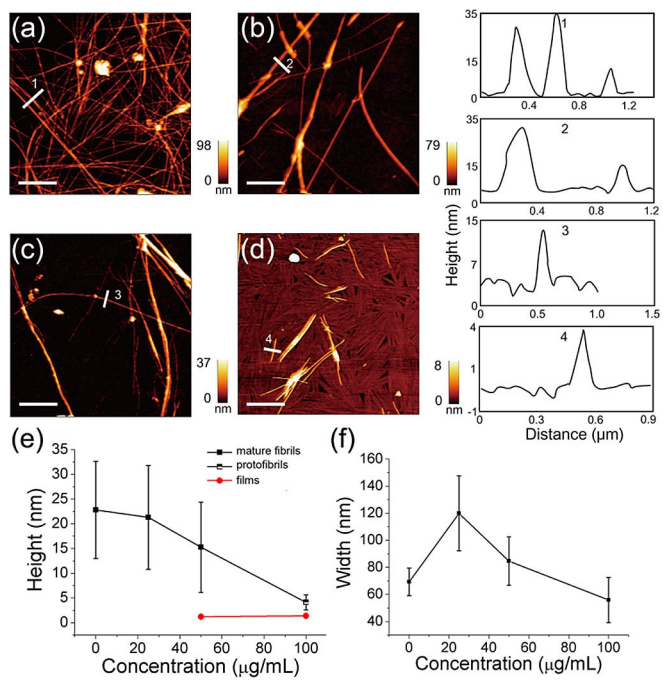

Figure 2. AFM images show MoS_2 modulation for amylin (20–29) aggregation. 550 μM amylin (20–29) peptide solution with 0 (a), 25 (b), 50 (c), and 100 μg mL^{-1} (d) MoS_2 were co-incubated for 10 h at 37 °C. The height of the fibrils were measured as 20 ± 4.5, 15 ± 3.7, 10 ± 2.7, and (2.3 ± 0.6) nm. The analyses for the fibril coverage show fibril height (e) and fibril width (f). The scale bar in the image is 2 μm.

lization of amylin (20–29) was faster to reach a saturation point at higher concentration (50 μg mL^{-1}), compared to its modulation on Aβ (33–42). In addition, we found the unstructured peptide film in the presence of MoS_2 at 50 μg mL^{-1} concentration. The measured height of unstructured peptide films was about 1 nm. The height of fibrils decreased from 20 to 2.3 nm with the concentration of MoS_2 shifting from 0 to 100 μg mL^{-1}. The linear fitting of fibril coverage versus the concentration of MoS_2 showed that the inhibition effect was efficient at lower concentrations, but it was gradually saturated with the increasing concentration (Figure S4). All the results implied that as the concentration of MoS_2 increased, fibrils tended to shrink and disappear, and peptide films formed. The modulation effect of MoS_2 on the self-assembly of amyloid peptides was investigated by QCM, a label-free detection method. The mixtures of 550 μM amyloid peptide and MoS_2 solution with different concentrations were pumped through the QCM chamber. The hybrids of peptides and MoS_2 adsorbed on the gold surface of QCM chip and induced a QCM frequency shift. Specifically 550 μM Aβ (33–42) or amylin (20–29) solution was mixed with 25 μg mL^{-1}, 50 μg mL^{-1}, or 100 μg mL^{-1} MoS_2 solutions. After that the mixture was pumped into QCM chamber and incubated for 10 h at 37 °C. Aβ (33–42) and amylin (20–29) peptides tended to adsorb onto the surface and gradually assemble into oligomer, and further into fibrils on the surface. As shown in Figure 3a and Figure 3b for Aβ (33–42), and Figure 3c and Figure 3d for amylin (20–29), the assembly process on gold surface consisted of a rapid growth (adsorption phase) and a slow rise (equilibrium reassembly phase). The shift of energy dissipation and the resonant frequency for Aβ (33–42) and amylin (20–29) are compared in Figure 3e. Different energy dissipation indicated the adhesion layers with different thicknesses and wet mass. The frequency shifts (ΔF_3) for the mixture of 550 μM Aβ (33–42) peptide solution and MoS_2 of 100 μg mL^{-1}, 50 μg mL^{-1}, 25 μg mL^{-1}, and 0 μg mL^{-1} were -0.6 ± 0.3 Hz, -3.9 ± 0.2 Hz, -16.0 ± 2.1 Hz and -20.4 ± 4.3 Hz, respectively; whereas the energy dissipation (ΔD_3) values were $7.8 \pm 1.0 \times 10^{-6}$, $18.5 \pm 2.5 \times 10^{-6}$, $27.0 \pm 3.2 \times 10^{-6}$, and $31.7 \pm 4.9 \times 10^{-6}$, respectively. A similar tendency was observed for 550 μM amylin (20–29) peptide solution mixed with MoS_2. The ΔF_3 for the mixtures of 550 μM amylin (20–29) peptide solution and MoS_2 of 100 μg mL^{-1}, 50 μg mL^{-1}, 25 μg mL^{-1}, and 0 μg mL^{-1} were -0.1 ± 0.2 Hz, -2.4 ± 0.7 Hz, -8.5 ± 1.7 Hz and -18.5 ± 3.4 Hz, respectively. The ΔD_3 vales were $1.8 \pm 0.8 \times 10^{-6}$, $2.3 \pm 0.9 \times 10^{-6}$, $6.1 \pm 1.8 \times 10^{-6}$ and $13.2 \pm 2.5 \times 10^{-6}$, respectively. The QCM frequency shift decreased with increasing concentration of MoS_2 from 25 to 100 μg mL^{-1}. The stronger inhibition effect of MoS_2 on the aggregation of amyloid peptides correlated with the higher concentration of MoS_2.

In addition, the secondary structure of amyloid peptide is the determinant feature for the formation of amyloid fibrils. We evaluated the secondary-structure change of Aβ (33–42)

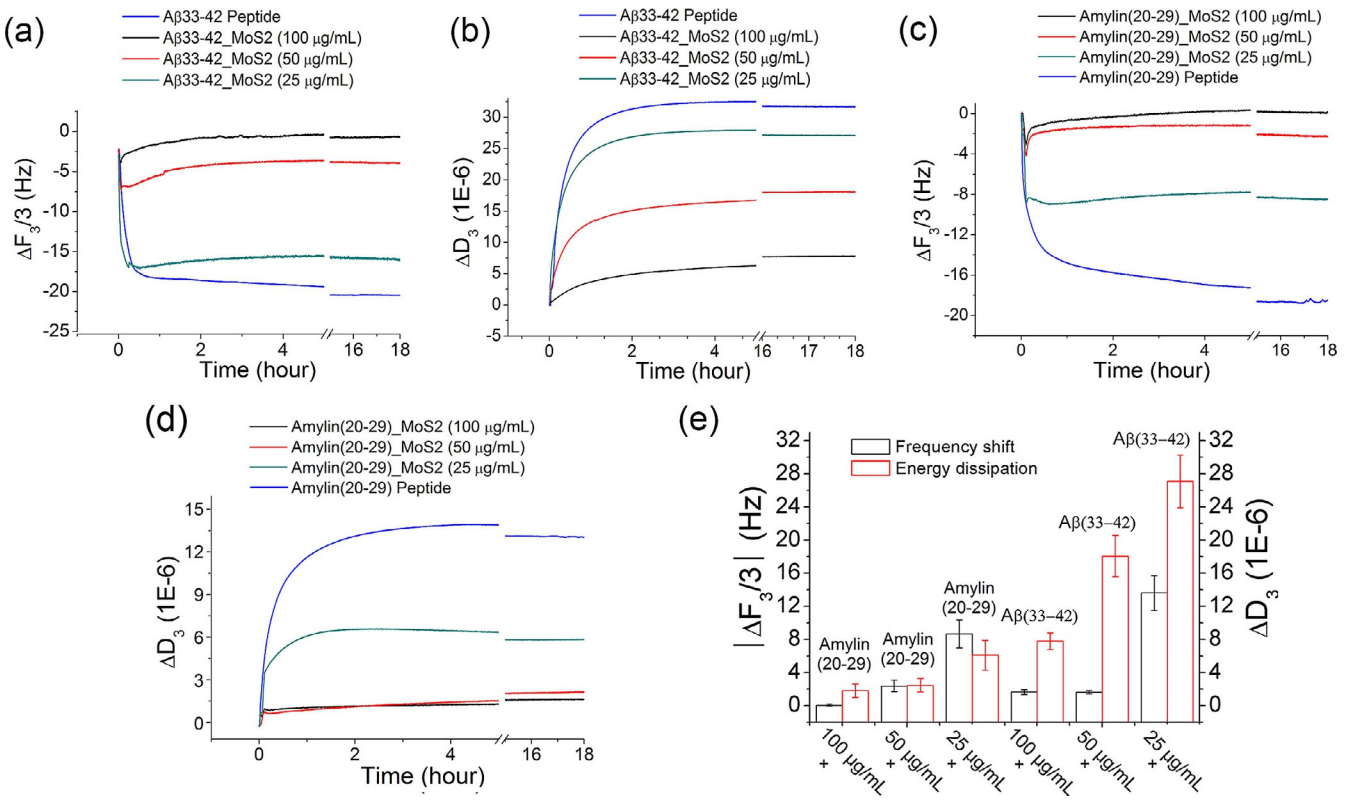

Figure 3. QCM monitoring of the modulation effect of MoS_2 on the assembling dynamics of Aβ (33–42) and amylin (20–29). a) The frequency-shift curve (ΔF3) and b) the energy dissipation curve (ΔD3) for 550 μM Aβ (33–42) peptide solution mixed with 25 μg mL^{-1}, 50 μg mL^{-1}, and 100 μg mL^{-1}, MoS_2 for 10 h at 37 °C; c) the frequency-shift curve (ΔF3) and (d) The energy dissipation curve (ΔD3) for 550 μM amylin (20–29) peptide solution mixed with 25 μg mL^{-1}, 50 μg mL^{-1}, and 100 μg mL^{-1} MoS_2 for 10 h at 37 °C; e) energy dissipation versus frequency shift for amylin (20–29)/MoS_2 mixture and Aβ (33–42)/MoS_2 mixture.

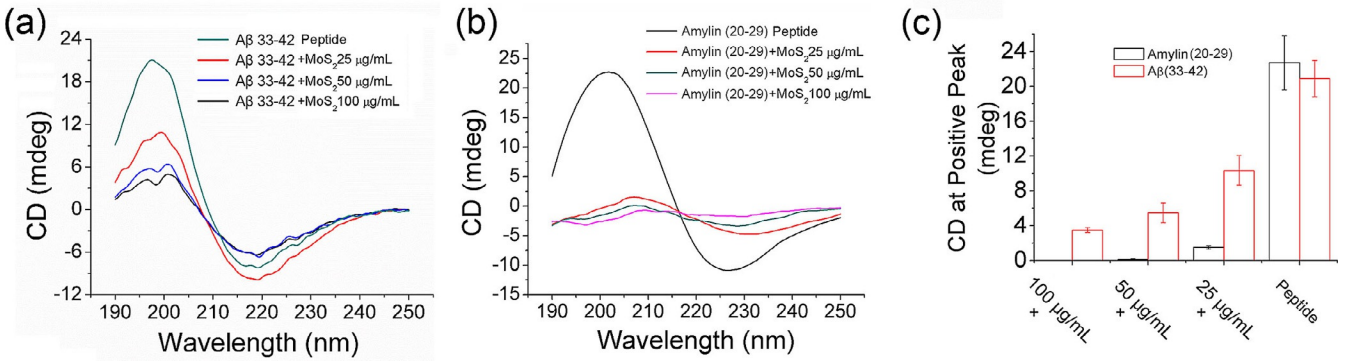

Figure 4. CD spectra of amyloid peptides modulated by MoS_2. a) The CD spectra of Aβ (33–42) modulated by MoS_2 at different concentrations. b) CD spectra of amylin (20–29) modulated by the MoS_2 at different concentrations. c) The CD signal of Aβ (33–42) at 198 nm and the CD signal of amylin (20–29) at 201 nm.

and amylin (20–29) in the aggregates influenced by MoS_2 by CD spectroscopy (Figure 4). We incubated the mixture solution of amyloid peptide and MoS_2 at 37 °C for 10 h and then measured the secondary structure of the peptides. As shown in Figure 4a, the typical β-sheet secondary structure of Aβ (33–42) was clearly observed in CD spectra (positive peak at 198 nm and negative peak at 218 nm),[18] and the typical β-sheet secondary structure of amylin (20–29) was also clearly confirmed by CD spectra (positive peak near 201 nm and negative peak near 230 nm),[19] as shown in Figure 4b. It was noteworthy that the intensity of CD signal representing β-sheet secondary structure decreased with the concentration of MoS_2 increasing from 0 to 100 $\mu g\,mL^{-1}$ for both Aβ (33–42) and amylin (20–29) peptides. The CD signals of Aβ (33–42) and of amylin (20–29) at positive peaks were compared (Figure 4c), suggesting that less amyloid peptide assemblies with β-sheet secondary structure formed upon interference with MoS_2.

To further explore and compare the modulating effect of MoS_2 on the aggregation of Aβ (33–42) and amylin (20–29), we systematically analyzed and calculated the modulation efficacy of MoS_2 on amyloid peptide aggregation, combining QCM, AFM, and CD results using Equation (1):

$$\text{Modulationefficacy} = \left(1 - \frac{\Delta\text{sample}}{\Delta\text{peptide}}\right) \times 100\% \quad (1)$$

where Δsample denotes the frequency shift in QCM result or the fibrils coverage in AFM or the intensity of positive peak signal of CD spectrum; Δpeptide represents the signal of the peptide without the interference of MoS_2 serving as positive controls. The calculation results were concluded in Table S1. It was obviously illustrated that the inhibitory effect of MoS_2 on amylin (20–29) aggregation was stronger than on Aβ (33–42) aggregation, especially at the lower concentration of MoS_2. The similar differential modulating effect of MoS_2 on the amyloid assembly was also observed and revealed at the early events of amyloid fibril formation, for example after 3 h (Figures S5 and S6). The inhibitory efficacy illustrated the efficacy of MoS_2 was higher on amylin (20–29) than that on Aβ (33–42), and the trend of inhibitory efficacy was consistent with the result obtained at time point of 10 h. In Figure S2, the CD signal of positive peak declined with an increasing concentration of MoS_2, which also illustrated the inhibiting effect of MoS_2 on the assembly of amyloid peptide after 3 h of treatment.

The modulation effect of MoS_2 on amyloid assemblies presented herein suggests the inhibition of the self-assembly of amyloid peptides.[20] MoS_2 can modulate the assembly of Aβ (33–42) more efficiently owing to the specific interaction and affinity between the Met (M) residue of peptide (NH_2-GLMVGGVVIA-COOH) and MoS_2. However, we noticed the more sensitive modulating effect of MoS_2 on the aggregation of amylin (20–29). Compared to Aβ (33–42), amylin (20–29) has more hydrophilic residues in the sequence (NH_2-SNNFGAILSS-COOH), a surfactant-like peptide (FGAIL is hydrophobic and SS is hydrophilic). Therefore the affinity between the peptide amylin (20–29) and MoS_2 is stronger than that between Aβ (33–42) and MoS_2, because amylin (20–29) has a similar amphipathic property to MoS_2, which confers strong affinity between them. The chemistry behind the modulating effect of MoS_2 is governed by the interaction between the peptide and MoS_2. The different affinities of peptides to MoS_2 result in the distinct modulating effects. One possible mechanism is proposed. The adsorption energy of amino acids to MoS_2 will determine the affinity of peptide to MoS_2. For Aβ (33–42), the sequence is NH_2-GLMVGGVVIA-COOH, and for amylin (20–29) the sequence is NH_2-SNNFGAILSS-COOH; we propose that the adsorption energy of S, N, and F to MoS_2 is much larger than those of M, V, and L, to MoS_2. Therefore, the affinity between the peptide amylin (20–29) and MoS_2 should be stronger than that between Aβ (33–42) and MoS_2, which might explain why MoS_2 exhibits a better modulating effect on the self-assembly of amylin (20–29) in comparison with Aβ (33–42).

In summary, we investigated the modulation effect of MoS_2 on amyloid peptide assemblies using a label-free method. MoS_2 was proven to modulate the Aβ (33–42) and amylin (20–29) assemblies in a concentration-dependent manner. Furthermore, the modulation effect of MoS_2 on amylin (20–29) assemblies was compared with the effect on Aβ (33–42) assemblies. This finding suggests MoS_2 is an effective modulator compara-

ble to graphene oxide as a promising 2D nanomaterial for amyloid peptide aggregation, which will enrich the category of the modulators of amyloid aggregation and extend the application of MoS_2 in biology.

Experimental Section

Preparation of Aβ (33–42) and amylin (20–29) solution and interaction with MoS_2

Amyloid peptide powder (2 mg; amino acid sequence: NH_2-GLMVGGVVIA-COOH; NH_2-SNNFGAILSS-COOH; Abbiochem Co., Ltd., China) were dissolved in 1 mL 1,1,1,3,3,3-hexafluoro-2-propanol (HFIP; Tokyo Chemical Industry, Japan), sonicated for 5 s, and vortexed for 5 s, repeating the sonication and vortex procedures for 3 times. Then the solution was kept in a thermo-shaker (PHMT, Grant Instruments, England) for 8 h at 350 rpm under 25 °C. Finally the solution was stored at −20 °C. Before use, 100 μL of Aβ (33–42) HFIP solution was transferred into a 1.5 mL centrifuge tube, and sealed with a piece of Parafilm. Then the tube was put in a vacuum drying oven (Jinghong Co., Ltd., China) for 1 h at 25 °C to completely evaporate the HFIP solvent. A thin film of peptide formed on the wall of tube. Afterwards, the peptide film in the tube was dissolved by adding Milli-Q water to form a peptide solution. Then, the solution was mixed with MoS_2 at room temperature. Then this mixture solution was sonicated for 5 s and vortexed for 5 s again, repeating the sonication and vortex procedures for 3 times until the solution was clear. Finally, the tube was placed on the thermo-shaker for 10 h at 350 rpm at 37 °C to generate the amyloid aggregate solutions used for analysis.

Atomic force microscopy

The peptide water solution was mixed with MoS_2 at room temperature. Then this mixture solution was sonicated for 5 s and vortexed for 5 s again, repeating the sonication and vortex steps for 3 times until the solution was clear. Finally, the tube was placed on the thermo-shaker for 10 h at 350 rpm at 37 °C. 20 μL mixture was taken out and deposited on the freshly cleaved mica for 10 min, after that the residue liquid on the surface was removed. The sample was rinsed once with Milli-Q water and dried under ambient conditions before the measurement. All AFM measurements were performed with a commercial AFM MFP-3D-SA (Asylum Research, Santa Barbara, California, USA) in tapping mode with ultrasharp silicon cantilevers (OMCL-AC160TS-R3; Olympus) and a nominal spring constant of 26 $N\,m^{-1}$. Resonant frequency was set at 300 kHz in all measurements. The scan frequency was set at 1 Hz with optimized feedback parameters. The resolution of all the original AFM images was 512×512 pixels. Muscovite mica freshly cleaved by adhesive tape was used as the substrate.

Raman spectroscopy

Raman measurements were performed by using a laser Raman spectrometer (DXR, Thermo Fisher, USA) at a wavelength of 532 nm. The laser power was set at 10 mW and a 50× objective lens was used to focus the laser beam on the sample.

Circular dichroism (CD) spectroscopy

CD spectra measurements were performed on a spectropolarimeter (JASCO, Hachioji City, Japan) with a model No. PTC-348W1 (JASCO). All experiments were performed at 25 °C, using a 0.1 cm quartz cuvette for spectral regions of 190–250 nm. Scan speed was set at 100 $nm\,min^{-1}$. The slit-width was set at 2 nm. For all samples, the signal of Milli-Q water was subtracted as the baseline. The sample volume for each CD measurement was 300 μL. All CD experiments were repeated 3 times($n = 3$).

Quartz crystal microbalance (QCM)

All of the QCM measurements were accomplished on a Q-Sense E4 (Biolin Scientific, Sweden). The solution of peptide or mixture consisting of amyloid peptide and MoS_2 was allowed to flow through the QCM chamber using a peristaltic pump at a speed of 50 $\mu L\,min^{-1}$. The hybrids of peptides and MoS_2 adsorbed and aggregated on the gold surface of QCM chip and induced the QCM frequency shift. All the QCM experiment was repeated for 3 times ($n = 3$).

X-ray diffraction

XRD was carried out on a Rigaku D/MAX-2500PC Diffractometer using Cu Kα radiation (I = 1.5406 Å). The scan angle is $5^\circ < 2\theta < 90^\circ$, in steps of 0.02°.

Acknowledgements

The authors gratefully acknowledge financial support from the Danish National Research Foundation, Aarhus Universitets Forskningsfond (AUFF NOVA-project), Karen Elise Jensens Fond, Villum Foundation, Lundbeck Foundation, EU H2020 RISE 2016 (MNR4SCell 734174 project). The authors gratefully acknowledge the financial support from national natural science foundation (21573097, 51503087). The authors also acknowledge the Foundation of Jiangsu Province (BK20140528, BK20140013, BK20140556, BK20150490, BK20160503) and the Foundation of Jiangsu University (Grant no. 14JDG021, 14JDG061 and 11JDG098), and the Foundation of Jiangsu Specially Appointed Professor. This work was also supported by Jiangsu Planned Projects for Postdoctoral Research Funds (1401068B). The authors gratefully acknowledge financial support from Senior Talent Start-up Funds of Jiangsu University (5503000004) and Jiangsu Postdoctoral Research Funds (1601118C).

Conflict of interest

The authors declare no conflict of interest.

Keywords: amyloid peptides · biophysics · fibrillogenesis · modulating assembly · molybdenum disulfide

[1] a) J. Hardy, D. J. Selkoe, *Science* **2002**, *297*, 353; b) G. S. Bloom, K. Ren, C. G. Glabe, *Biochim. Biophys. Acta* **2005**, *1739*, 116; c) C. C. Glabe, *Subcell. Biochem.* **2005**, *38*, 167.

[2] a) M. Zhang, X. Mao, Y. Yu, C. X. Wang, Y. L. Yang, C. Wang, *Adv. Mater.* **2013**, *25*, 3780; b) C. Li, R. Mezzenga, *Nanoscale* **2013**, *5*, 6207; c) T. Härd, C. J. Lendel, *Mol. Biol.* **2012**, *421*, 441; d) S. Butterfield, M. Hejjaoui, B. Fauvet, L. Awad, H. A. J. Lashuel, *Mol. Biol.* **2012**, *421*, 204.

[3] C. Cabaleiro-Lago, F. Quinlan-Pluck, I. Lynch, K. A. Dawson, S. Linse, *ACS Chem. Neurosci.* **2010**, *1*, 279.

[4] a) L. Liu, L. Niu, M. Xu, Q. Han, H. Duan, M. Dong, F. Besenbacher, C. Wang, Y. Yang, *ACS Nano* **2014**, *8*, 9503.

[5] a) C. Cabaleiro-Lago, I. Lynch, K. A. Dawson, S. Linse, *Langmuir* **2010**, *26*, 3453; b) M. Dong, M. Hovgaard, W. Mamdouh, S. Xu, D. Otzen, F. Besenbacher, *Nanotechnology* **2008**, *19*, 384013.

[6] a) J. Wang, Y. P. Cao, Q. Li, L. Liu, M. D. Dong, *Chem. Eur. J.* **2015**, *21*, 9632; b) J. Wang, Z. Zhu, C. Bortolini, S. V. Hoffmann, A. Amari, H. X. Zhang, L. Liu, M. D. Dong, *Nanotechnology* **2016**, *27*, 304001.

[7] a) S. Bag, R. Mitra, S. Dasgupta, S. Dasgupta, *J. Phys. Chem. B* **2017**, *121*, 5474 – 5482; b) H. Huang, P. Li, M. Zhang, Y. Yu, Y. Huang, H. Gu, C. Wang, Y. Yang, *Nanoscale* **2017**, *9*, 5044 – 5048; c) M. Yousaf, H. Huang, P. Li, C. Wang, Y. Yang, *ACS Chem. Neurosci.* **2017**, *8*, 1368 – 1377.

[8] a) M. Li, A. Zhao, K. Dong, W. Li, J. Ren, X. Qu, *Nano Res.* **2015**, *8*, 3216 – 3227; b) N. Kapil, A. Singh, M. Singh, D. Das, *Angew. Chem. Int. Ed.* **2016**, *55*, 7772 – 7776; *Angew. Chem.* **2016**, *128*, 7903 – 7907.

[9] a) Q. H. Wang, K. Kalantar-Zadeh, A. Kis, J. N. Coleman, M. S. Strano, *Nat. Nanotechnol.* **2012**, *7*, 699; b) A. Splendiani, L. Sun, Y. B. Zhang, T. S. Li, J. Kim, C. Y. Chim, G. Galli, F. Wang, *Nano Lett.* **2010**, *10*, 1271.

[10] B. Radisavljevic, A. Radenovic, J. Brivio, V. Giacometti, A. Kis, *Nat. Nanotechnol.* **2011**, *6*, 147.

[11] H. Zhang, S. B. Lu, J. Zheng, J. Du, S. C. Wen, D. Y. Tang, K. P. Loh, *Opt. Express* **2014**, *22*, 7249.

[12] a) S. G. Wang, K. Li, Y. Chen, H. R. Chen, M. Ma, J. W. Feng, Q. H. Zhao, J. L. Shi, *Biomaterials* **2015**, *39*, 206; b) S. G. Wang, Y. Chen, X. Li, W. Gao, L. L. Zhang, J. Liu, Y. Y. Zheng, H. R. Chen, J. L. Shi, *Adv. Mater.* **2015**, *27*, 7117; c) S. G. Wang, X. Li, Y. Chen, X. J. Cai, H. L. Yao, W. Gao, Y. Y. Zheng, X. An, J. L. Shi, H. R. Chen, *Adv. Mater.* **2015**, *27*, 2775.

[13] a) A. Noormägi, K. Primar, V. Tougu, P. J. Palumaa, *Pept. Sci.* **2012**, *18*, 59; b) I. Nasir, S. Linse, C. Cabaleiro-Lago, *ACS Chem. Neurosci.* **2015**, *6*, 1436; c) S. A. Hudson, H. Ecroyd, T. W. Kee, J. A. Carver, *FEBS J.* **2009**, *276*, 5960; d) A. K. Buell, C. M. Dobson, T. P. J. Knowles, M. E. Welland, *Biophys. J.* **2010**, *99*, 3492.

[14] L. Liu, L. Zhang, X. B. Mao, L. Niu, Y. L. Yang, C. Wang, *Nano Lett.* **2009**, *9*, 4066.

[15] S. Zhang, M. Andreasen, J. T. Nielsen, L. Liu, E. H. Nielsen, J. Song, G. Ji, F. Sun, T. Skrydstrup, F. Besenbacher, N. C. Nielsen, D. E. Otzen, M. D. Dong, *Proc. Natl. Acad. Sci. USA* **2013**, *110*, 2798.

[16] H. S. S. Ramakrishna Matte, A. Gomathi, A. K. Manna, D. J. Late, R. Datta, S. K. Pati, C. N. R. Rao, *Angew. Chem. Int. Ed.* **2010**, *49*, 4059 – 4062; *Angew. Chem.* **2010**, *122*, 4153 – 4156.

[17] H. Li, Q. Zhang, C. C. R. Yap, B. K. Tay, T. H. T. Edwin, A. Olivier, D. Baillargeat, *Adv. Funct. Mater.* **2012**, *22*, 1385.

[18] Y. Guo, J. Wang, *ChemPhysChem* **2012**, *13*, 3901.

[19] R. C. Elgersma, G. E. Mulder, J. A. Kruijtzer, G. Posthuma, D. T. Rijkers, R. M. Liskamp, *Bioorg. Med. Chem. Lett.* **2007**, *17*, 1837.

[20] P. K. Chow, E. Singh, B. C. Viana, J. Gao, J. Luo, J. Li, Z. Lin, A. L. Elias, Y. F. Shi, Z. K. Wang, M. Terrones, N. Koratkar, *ACS Nano* **2015**, *9*, 3023.